Improving the compressive response of bio-polymeric additively manufactured cellular structures via foam-filling: An experimental and numerical investigation

Improving the Compressive Response of Bio-Polymeric Additively Manufactured Cellular Structures via Foam-Filling: An Experimental and Numerical Investigation

A. Corvi, L. Collini*, C. Sciancalepore

Department of Engineering and Architecture, Parco Area delle Scienze 181/A, 43124 Parma (IT)

alberto.corvi@unipr.it; luca.collini@unipr.it; corrado.sciancalepore@unipr.it

ABSTRACT

Additive Manufacturing recently answers the need of advanced innovative designs for functional applications. Lattice structures and lightweight composites are the result of engineered designs for enhanced mechanical, structural and energetic properties. Inspired by nature, this work investigates the static and cyclic compressive response of 3D-printed TPMS-cellular structures in Poly-(Butylene-Adipate-*co*-Terephthalate) (PBAT) bio-polymer, functionalized with Poly-Urethane foam. The plateau stress of the hybrid structure is 30% increased and its specific energy absorption capability 18% enhanced, due to the "interaction effect" between the two phases. An accurate Finite-Elements model is developed as a supporting tool to analyze, predict, and optimize the structure behavior, together with a deeper understanding of the deformation mechanism of such structures. In addition, PBAT is proved to be the ideal candidate for a greener manufacturing, combining good mechanical property with its characteristic biodegradability, paving the pathway for new fields of application.

Keywords: *Cellular Structures; Energy Absorption; FDM Additive Manufacturing; Multi-phase Mechanical Metamaterials; Foam-filling.*

*Corresponding author: luca.collini@unipr.it

1. INTRODUCTION

Additive Manufacturing (AM) has recently achieved a key role in producing advanced structures, thanks to its capability to embrace complex designs otherwise impossible to obtain with traditional subtractive or formative technologies. Lattices and Triply Periodic Minimal Surface (TPMS) structures, often referred to in literature as Mechanical Metamaterials (MM), are the result of this capability of re-designing structural and functional components to obtain superior properties [1-3]. In the last years, lightweight structures with enhanced mechanical behavior paved the way for new multifunctional applications in many engineering fields, such as biomechanical [4-5], aerospace, acoustic [6] and energy storage [7-9]. Following this, numerical tools aiding in the design and structural optimization have become of primary importance thanks to their facilitating role both in adopting a highly innovative design [10] and in predicting the structure engineering behavior [11].

Among AM technologies, the most widely employed is commercially known as Fused Deposition Modeling (FDM), consisting in the extrusion and consequent deposition of a polymeric filament in a semi-melted status: Lattices and TPMS structures have attracted increasing attention also in the FDM world, related with thermoplastic polymers. In this framework, the main applications concern the compressive behavior [3, 12-15], with a wide range of practical employs ranging from lifestyle products [16] to engineering crashworthy components [17-19].

Focusing on the structure energy absorption feature, the use of a secondary material, typically foam-like, is often employed to enhance the mechanical response of the structure under compressive loads, as shown in literature [20-24]. Roudbeneh [25] proved an energy absorption increase up to 50% for PU-filled honeycomb sandwich panels and a substantial beneficial effect related with the damage appearance. Other filler materials recently investigated are gels [26-27], proving an enhanced energy absorption capability, water [28], demonstrating a damping effect during impact loadings, and shear-thickening-fluids [29] allowing to create a dynamic response depending on the fluid shear rate, i.e. on the interaction between geometry and fluid as function of the impact velocity. Poly-Urethane (PU) foams are for sure the most important portion among polymeric foams: their remarkable lightweight is

combined with promising thermo-mechanical properties, making them ideal candidates as thermal and sound insulators, as well as useful materials for advanced mechanical applications [30-31].

The technique of foam-filling a thin-walled structure with PU foam is often related with a significant increase in the energy absorption capability of the assembly: Yao [32] and Ren [33] reported the beneficial interactive effect between the foam and the external shell, aluminum and stainless-steel auxetic tubes, respectively, noticing a significantly improved response if compared to the algebraic sum of the contributions of single constituents. Recently, 3D-printed lattice structures have been also foam-filled, combining the effect of a novel designed or optimized structure with that of the filler [34-36]. Miralbes [37] compared the experimental responses of different TPMSs with the hybrid (foam-filled) configuration, finding out the foam delays the appearance of densification regime at higher strains and reduces the layer-by-layer failure of the structure. Also, the effect of foam-filling cellular structures via a multi-material-AM technique has been experimentally investigated in [38], showing enhanced stiffness and energy dissipation compared to empty and equivalent-weight structures. However, these encouraging findings are related to experimental evidence and lack a deeper investigation on the deformation mechanism of such structures.

In this framework, the present work provides a deeper understanding of the deformation mechanism of such structures, and discusses the possible tools to analyze and improve their functional performances. A PBAT 3D-printed walled cellular structure is investigated under static and cyclic compressive loadings within two configurations, empty and filled with PU foam. Focus is set on the stress field developed during compression, and the consequent global deformation of the structure, responsible of its overall mechanical performance. Also, the enhanced energy absorption capability for the PU-filled scenario is discussed, related with the interactive effect between the two constituent phases: this latter interesting phenomenon beneficially influences the resulting performance. A Finite-Element (FE) model is developed as a tool to better understand the stress distribution in the structure: simulation outputs are compared with experimental data, both in resulting mechanical response and in structure deformation, providing an accurate match.

Moreover, a novel material is introduced in the engineering world: a non-commercial filament of Poly-(Butylene Adipate-*co*-Terephthalate) (PBAT) biopolymer is extruded and FDM-printed. Thanks to its promising properties, PBAT is the optimal candidate to produce components that combine good mechanical performances with both new fields of applications [39] and the attention to a more environmentally friendly production [40]. In fact, PBAT is a thermoplastic polyester that is gaining significative importance due to its biodegradability in conjunction with good mechanical properties: high flexibility and relatively low elastic modulus make PBAT easily processable as filaments to produce very flexible parts by 3D printing, replacing the non-degradable oil-derived flexible filaments currently commercially available.

2. MATERIALS & METHODS

2.1 Structure geometry

The inspiration for this work is found in the natural world, where structures with multifunctional properties are the result of adaptation of the species over millions of years. When the focus is pointed on energy absorption properties, as for example in the turtle shell or in the woodpecker skull, the use of a secondary material, typically foam-like, is often involved to enhance the mechanical response of the structure, see Figure 1a. More in details, Schwarz primitive lattice (P-lattice) geometry is taken into numerical environment, and from that a unit cell of 10x10x10 mm is obtained providing an outwards shell thickness of 0.8 mm. The periodic structure is created via a face-to-face tessellation of the previously defined unit cell, as resumed in Figure 1b. External walls are added to the resulting structure, again with 0.8 mm of thickness, to generate a close volume suitable to be filled with a secondary material.

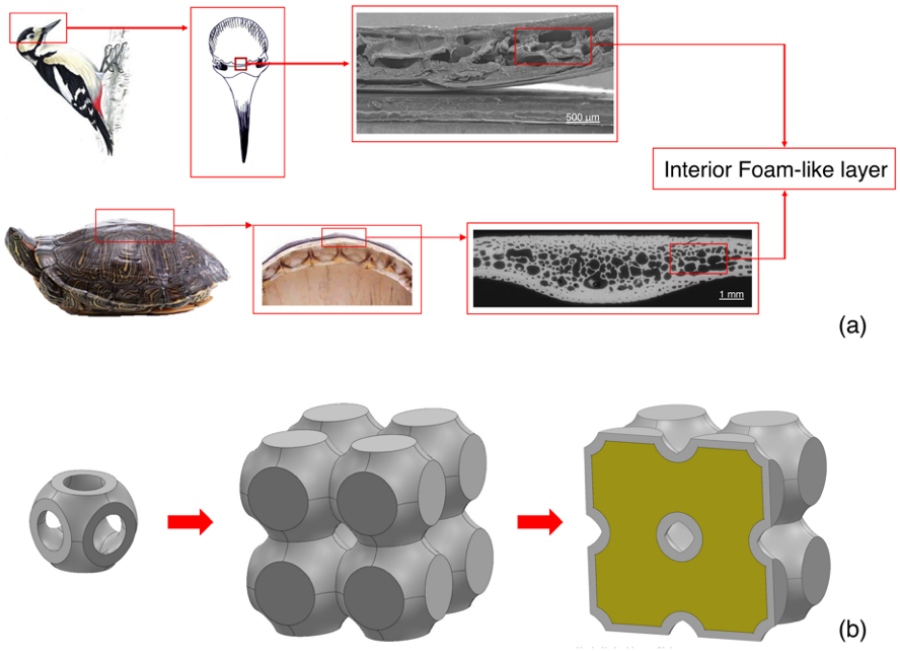

Figure 1: a) Bio-inspiration for multiphase composites for enhanced energy absorption; b) Structure definition via tessellation of unit cell and addition of walls.

Specimens of 2x2x2 array of cells are printed, with the aim of trading-off the printing time, which is of the order of 2.5-3 hours: the specimen representativity for a periodic arrangement is investigated in Section 3.3, where two specimens of 3x3x3 array of cells are also printed and tested for a scaling effect.

The value of relative density ϕ, which is the most significant parameter when designing cellular and lattice structures, is controlled by means of Eq. (1) and falls inside the range proposed by Ashby [41], where the "cellular solids" nature is defined for $\phi < 0.3$.

$$\phi = \frac{\rho^*}{\rho_s} = \frac{\rho_{lattice}}{\rho_{solid}} = 0.26 \tag{1}$$

2.2 Materials characterization

PBAT is a semicrystalline thermoplastic polymer, characterized by a significant ductile and stretchy behavior. Its biodegradability is giving it an emerging position as the preeminent flexible bioplastic [42]. PBAT combines some of the beneficial

attributes of synthetic and bio-based polymers: it is derived from common petrochemicals and yet it is biodegradable. It is composed of two repeating units: butylene terephthalate (BT) and butylene adipate (BA), linked together by a condensation reaction; the properties of the copolymer are dependent of the molar ratio of these constituents. As a synthetic polymer, it can readily be produced at large scale, and it has the physical properties needed to make flexible films that rival those from conventional plastics [43].

Thanks to its encouraging properties, PBAT has recently been introduced in the 3D-printing world. In this work, the PBAT pellets, bought from MAgMa Spa (Italy) as white granules (PBAT Ecoworld), are used to create a filament suitable for the printing by means of a single screw extruder (Felfil Evo, Felfil, Italy). The system includes multiple fans, to cool down the polymer, and a spooler, to regularize the diameter of the obtained filament to a constant value via an optical sensor, as shown in Figure 2. The extrusion temperature is set at 150 ± 10 °C and the screw angular velocity is maintained at 3 rpm. The target value for the filament diameter is fixed at 1.65 ± 0.10 mm.

The BQ Hephestos-2 3D printer was used with the following printing parameters: the temperature of the printer's head was set at 180 °C; the printing velocity was 20 mm/s; the diameter of the extruder nozzle is 0.6 mm and the layer height is 0.2 mm.

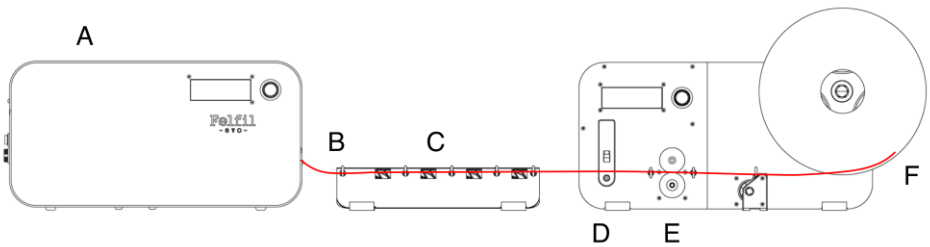

Figure 2: PBAT extrusion line scheme: A – extruder; B – wire extrusion head; C – air cooling system; D - optical sensor; E - filament pull spools; F - filament winder.

FDM-printed specimens, with standard UNI EN ISO 527 and 1BA geometry, underwent a uniaxial tensile test on TesT dynamometer (Model 112, 2kN cell load, TesT GMBH Universal Testing Machine, Germany) with a cross-head velocity of 50 mm/min: the aim is to obtain the mechanical characterization of the 3D printed

material. The material behavior is reported in Figure 3a, showing an initial linear elastic response, until the yielding threshold is reached; at larger strain, a wide plastic "plateau" region followed.

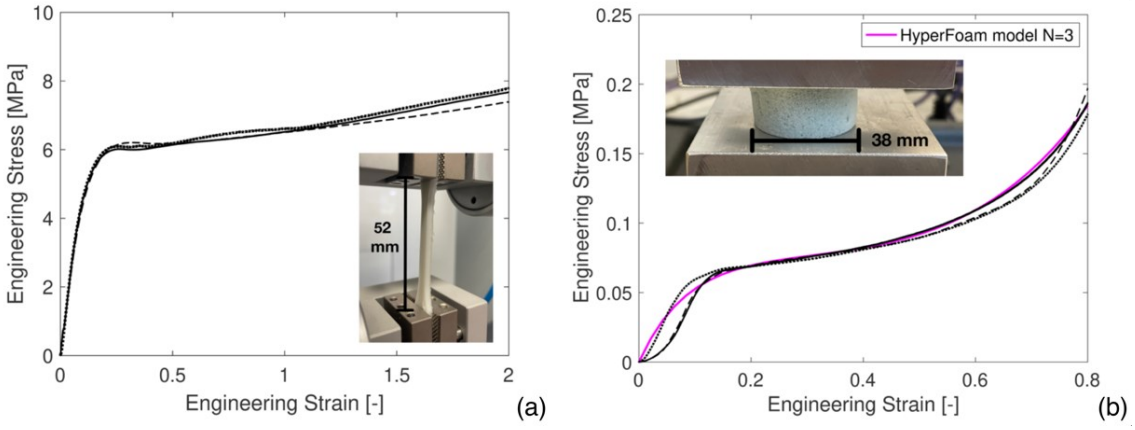

Figure 3: a) Tensile response of 3D-printed PBAT; b) Compressive behavior of PU foam.

Regarding the foam, a commercial PU-foam was employed. The density has been experimentally determined as $\rho_{foam} = 47.2\, Kg/m^3$. Moreover, to characterize the foam response, cylindrical samples of foam have been tested in compression, with height/radius ratio $H/R = 1$ and dimensions suitable to consider the porosity homogeneous inside the sample. Resulting curves are reported in Figure 3b.

2.3 Numerical modelling

A Finite-Elements (FE) model is developed within the commercial software Abaqus© to simulate the mechanical response of the structure: from that the numerical outputs in terms of macro-scale deformation and load-displacement curve are compared with the experimental compressive behavior. PBAT has been modelled via an elasto-plastic constitutive model, according with what previously discussed in paragraph 2.2: Young modulus of $E = 60MPa$, Poisson ratio of $\nu = 0.46$ computed by a Digital Image Correlation (DIC) analysis, and plastic regime defined through test data from Figure 3a, are numerically set. Regarding PU-foam, its behavior is noticed to be hyper-elastic, and so it is modelled via the HyperFoam constitutive model, in which the strain energy density function U is expressed in terms of the principal stretches, as reported in Eq. (2). A numerical fitting between test data and the

numerical model is performed in Abaqus© environment: an HyperFoam model of 3rd degree is found to be the most accurate model, see Figure 3b. In. Table 1 lists the coefficients employed for the simulations, with β representing the compressibility of the foam defined as: $\beta = \nu/(1-2\nu)$.

$$U = \sum_{i=1}^{N} \frac{2\mu_i}{{\alpha_i}^2}\left[\hat{\lambda}_1^{\alpha_i} + \hat{\lambda}_2^{\alpha_i} + \hat{\lambda}_3^{\alpha_i} - 3 + \frac{1}{\beta}\left({J_{el}}^{-\alpha_i\beta} - 1\right)\right] \quad (2)$$

Table 1: Coefficients for HyperFoam model

	μ_i	α_i	β
$i=1$	-0.200436	9.09239	
$i=2$	0.205346	9.09473	1.16666
$i=3$	0.443730	-9.14177	

The analysis is performed in Abaqus/Explicit environment. **General Contact* is used, considering both the contact between the top and bottom faces and the plates and the contact of the structure with itself during the compression process; "hard contact" is defined in the normal direction while the tangential behavior is modelled with "penalty" function and 0.2 friction coefficient. Both plates (upper and lower) are modelled via analytical rigid surfaces. Linear C3D4 elements are adopted, with proper size suitable to consider the mesh-independence after a convergence analysis, in Fig. 4a. Mass scaling with a factor of 10 is employed in the whole model to scale the minimum solution increment with no loss of physical meaning. A **TIE* constraint, in Fig.4b, is set between the cell internal surface and the external of the foam: in this way, any detachment between the shell and the foam is avoided. This finds evidence in experiments, as a specimen has been cut in half after being deformed and perfect adhesion is noticed.

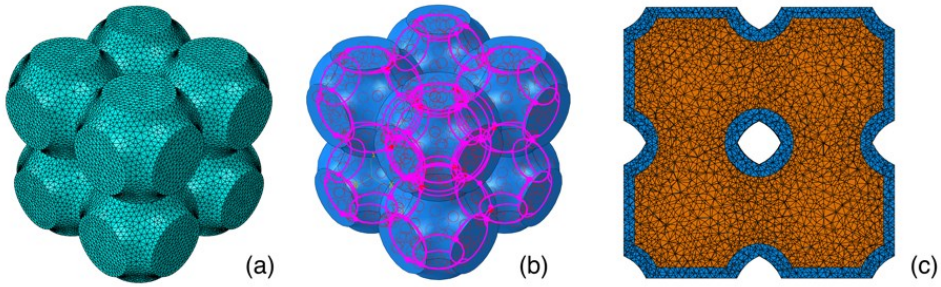

*Figure 4: Numerical model: a) Mesh of the external shell; b) *Tie constraint between shell and foam; c) Foam mesh.*

2.4 Performance parameters

Both empty and Foam-Filled (FF) configurations have been tested, experimentally and numerically, under compression loading with a displacement rate of 5 mm/min [33], and resulting curves are compared to appreciate the foam contribution on the load-carrying capacity. Cyclic loading has been also applied to investigate the transient behavior of the material. The total energy absorption (TEA) and the total energy dissipation (TED) capabilities are defined as in Eq. (3), where F represents the applied load and x_0 and x_f the displacement at the first and final stage, respectively:

$$TEA = \int_{x_0}^{x_f} F(x)dx \qquad TED = \oint_{x_0}^{x_f} F(x)dx \tag{3}$$

To compare the two configurations, it is necessary to introduce the absorbed and dissipated energy per unit of mass, i.e. specific energy absorbtion (SEA) and dissipation (SED), and the damping capacity per unit of mass, i.e. specific damping capacity (SDC), evaluated in Eq. (4):

$$SEA = \frac{TEA}{M} \qquad SED = \frac{TED}{M} \qquad SDC = \frac{TED}{TEA} \tag{4}$$

The stress analysis of thin-walled structures can be approached adopting the stress linearization technique. To compute the linearization, the stress field over defined

sections is considered. These sections are referred to as stress classification planes (SCPs). The limit for two opposite sides of an SCP with infinitesimal distance between them is a Stress Classification Line (SCL): SCLs are straight lines that cut through a section of a component.

This study embraces the Structural Stress Method, being the most frequently adopted technique for stress linearization. In this method, stress components are integrated along SCLs through the wall thickness, *t*, to determine the membrane and bending stress components, defined as follows:

$$\sigma^m = \frac{1}{t}\int_{-t/2}^{t/2} \sigma \, dx \qquad \sigma^b = \frac{6}{t^2}\int_{-t/2}^{t/2} \sigma \, x \, dx \tag{5}$$

2.5 Sample representativity

Being the considered solid a cellular structure based on a spatial face-to-face tassellation of a unit cell, it is primarly important to discuss the scalability of the findings. In other words, it is necessary to verify that the considered configuration is a significant reference volume to describe the response of a much bigger component in real applications. Carrying out experimental tests, it is not possible to be sure about the error in neglecting any border effects combined with a finite geometry. To this aim, a validation method has been developed based on a double check while testing structures with varying cell layers. The check is made on:

i) the increase of the energy dissipation capability due to the foam is compared among tests;

ii) the elastic response of the structure is studied to check if any significant anomaly occurs.

To obtain the stress-strain curve of the overall compressive response, the nominal compressive stress $\sigma_{N,c}$ and the nominal compressive strain $\varepsilon_{N,c}$ are to be defined:

$$\varepsilon_{N,c} = \frac{-u_c}{h_0} \qquad \sigma_{N,c} = \frac{P_c}{A_{0,eq}} \tag{6}$$

where P_c is the compressive load, u_c is the nominal displacement, h_0 the initial height of the structure. $A_{0,eq}$ represents the equivalent cross-section area of the structure, described as in Eq. (7), where V_L is the volume of the lattice structure:

$$A_{0,eq} = \frac{V_L}{h_0} = \phi \cdot {h_0}^2 \tag{7}$$

The initial stiffness K_0 of structures with different sizes is also computed, to check if the macro-scale elasticity does not provide remarkable differences, admitting to state the correct scalability of the examined structure. To obtain the initial stiffness, the crosshead displacement of the test machine along the z-direction and the reaction forces measured by the loading cell are considered:

$$K_0 = \left.\frac{dF_T(z)}{dz}\right|_{(\varepsilon=0.05)} \tag{8}$$

where F_T is the total load during the test. The differentiation of the function $F_T(z)$ has been computed from 0.05 strain on, i.e. neglecting the initial part where the elastic behavior is not linear because of inaccuracies in the sample geometry due to the printing process.

3. RESULTS AND DISCUSSION

3.1 Static loading and stress field investigation

The behavior under static compression is shown in Fig. 5a, up to 65% of compression for the original and the FF configurations. Numerical simulations are also plotted. The FF technique proved to induce an increase in the load-carrying capacity at the end of the initial linear response. At small values of compression, the foam resistance is negligible, according to its hyper-elastic behavior, whereas at increasing

compression the shift between empty and FF responses becomes significant, with the latter characterized by a higher load carrying capacity over the plateau region. In this range of deformation, the empty configuration shows an unsteady fluctuating curve, because of subsequent instabilities occurring in the cell walls; on the other hand, the foam produces an almost uniform behavior, stabilizing the load approximately between 25% and 50% of strain.

The match of load-displacement curve between the FE simulation and experimental tests looks accurate, allowing to successfully validate the numerical model. Also, the deformation of the structure is well reproduced by the simulation output, as reported in Fig. 5b which shows the stress distribution in both configurations at nominal compression 0%, 15%, 27%, 35% and 40%. Indeed, the structure undergoes a very different deformation field in the two tested configurations: observing the deformed configurations, the PU foam acts as a constraint for the transverse displacement, preventing the inward/outward bending of the cell wall. According with this, the stress distribution in the external wall is also very different. In particular, filling the inner cavity with the foam generates an overall regular deformation of the structure, also in correspondence of significant levels of compression: hence, a more isotropic stress distribution in the wall is reached.

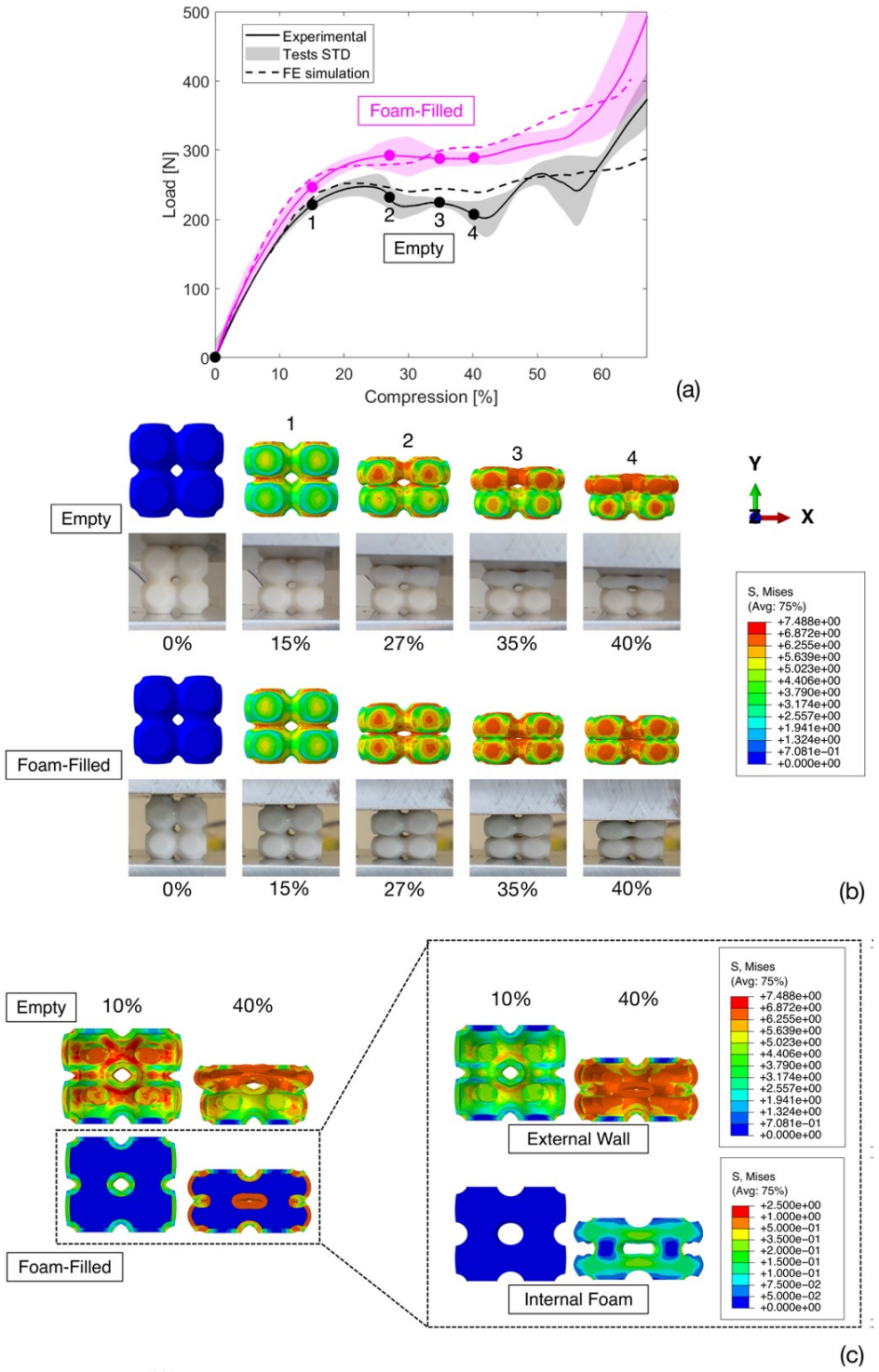

Figure 5: a) Quasi-static compression of empty and FF configurations; b) Stress distribution at different levels of compression; c) Wall and foam contributions.

Besides, the empty configuration is severely affected by the collapse of the upper layer of cells, that completely loses its load-bearing capacity while the bottom layer is only slightly deformed. The anisotropy reduction due to the foam presence is clearly

visible in Fig. 6, in which the axial stress of the two layers of cells are compared for incresing levels of nominal compression, proving that the benefits of the filling technique are much more meaningful than the foam contribution itself which is almost two orders of magnitude smaller than that of the wall, as evindenced before in Fig. 5c.

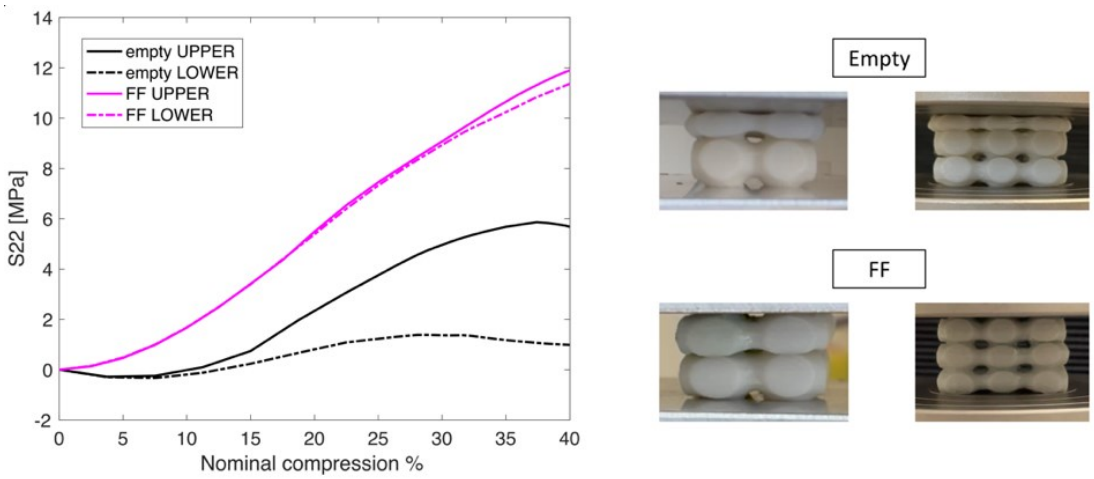

Figure 6: Regularization of the stress field and deformation thanks to the foam filling.

To deeply understand the stress distribution on the structure and the influence of the foam in local regions of the stress field, a path is defined through the wall thickness at the center of the external closing walls, see Fig. 7a, i.e. where the maximum value of stress is reached. Figure 7b shows that, while for small levels of nominal compression the stress distribution between empty and FF configurations is almost the same, for higher values (35% of nominal compression) the difference become significant, according to the different macroscopic deformation of the structure previously discussed (see Fig. 6).

Fig. 7c compares the upper and lower layers at 35% of nominal compression, providing data to support the stress regularization effect consequent to the smoothing of deformation distribution experimentally evidenced. In particular, focusing on the continue red line referring to the axial stress in the upper layer, it is noticed how for the FF configuration the walls undergo an only compressive stress (from 0 to -5 MPa) while for the empty configuration the stress state is bending and with a much more significant gradient (+4 MPa and -12 MPa at the boundaries of the path).

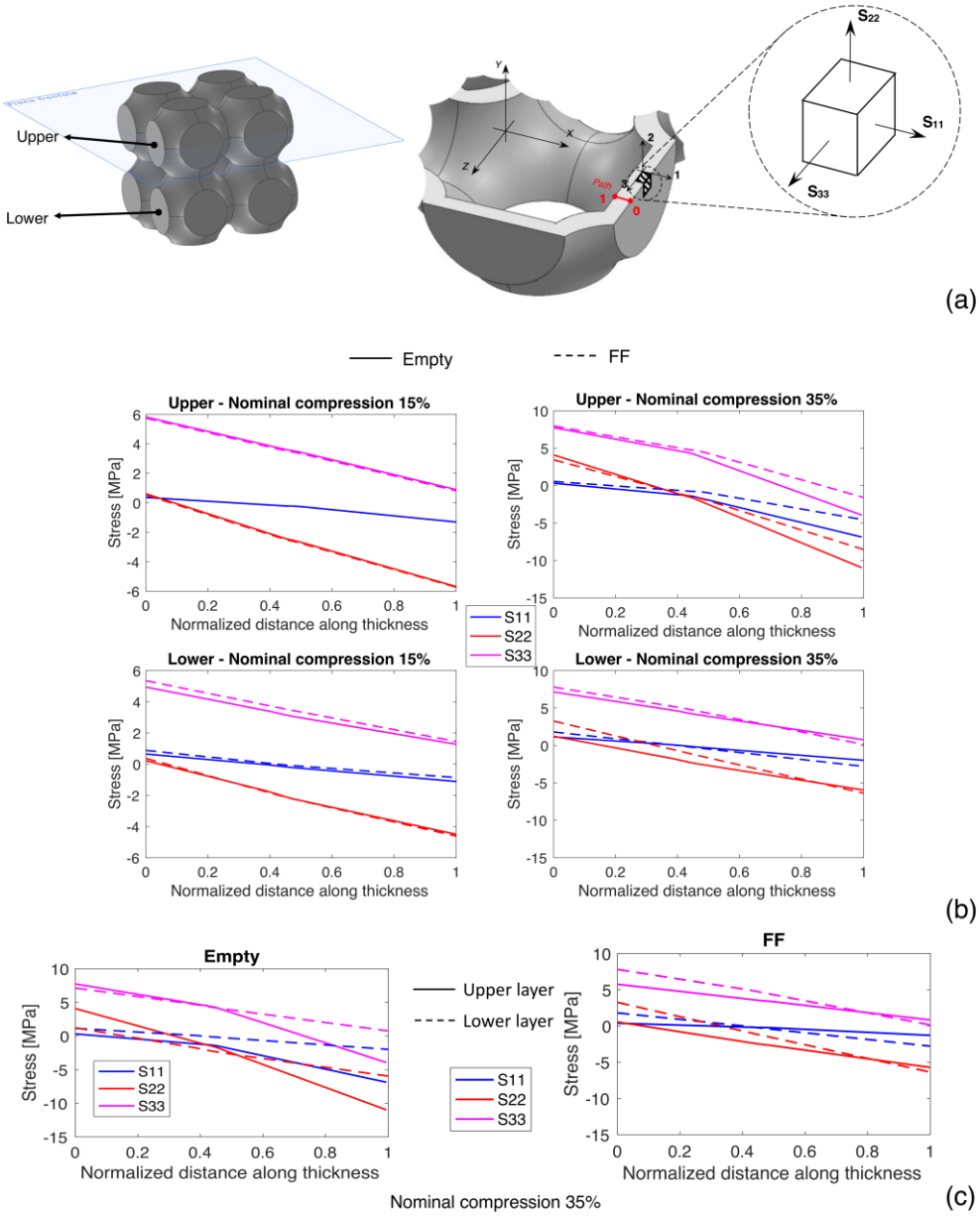

Figure 7: a) Path along wall thickness; b) Comparison of the stress distribution along path at different levels of nominal compression; c) Foam effect on the stress regularization.

3.2 Energy absorption performances

Filling the structure with a secondary soft material does not produce only an increase in the overall compressive response: the effect of the foam on the more isotropic response at the macro-scale has been discussed in paragraph 3.1. Together with this beneficial effect, the TEA (and so also the TED) of the FF configuration is noticed to be much higher than the algebraic sum of the separate contributions from

the individual constituents, PBAT and PU foam. This phenomenon is also observed in [32-33], justifying the choice of foam-filling the structure. The green area in Fig. 8a and 8b shows the significance of the interaction effect between the wall and the foam exhibited by the FF structure. The reason for this peculiar behaviour is found again in the more regular deformation during compression: the foam inside, subjected to compressive stresses, can indeed prevent some instability phenomena, leading to a deformation mode that limitates the buckling appearance, resulting also in a more stable mechanical response. Again, the FF load-displacement curve presents a linear "plateau" region, contrarily to what observed for the empty configuration: the reason for this is that the irregular behavior of the empty structure is due to instabilities phenomena of consequent layers. Thus, more than load carrier, again the soft filler acts as regularizer of the behaviour of the stronger scaffold.

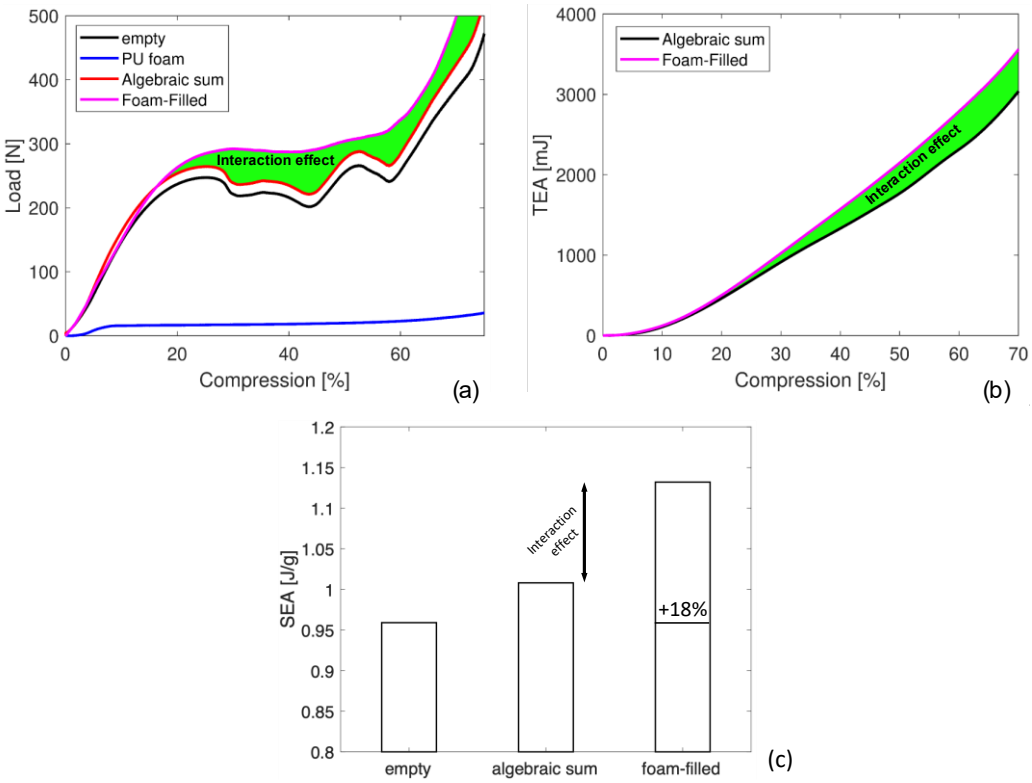

Figure 8: Interaction effect between the external structure and the foam: a) Increased compressive response; b) Enhanced total energy absorbtion; c) Comparison of the specific energy absorption.

A comparison of the specific energy absorption is shown in Fig. 8c: the FF configuration presents a +18% increase in the SEA capability compared to the non-hybrid configuration. This encouraging result is mainly due to the interaction effect between the two phases, significantly evidenced in Fig 8c.

In the cyclic loading testing, both empty and FF configurations underwent compressions up to 75% of nominal height, with the same test parameters of the quasi-static monotonic test. The TED previously defined in Eq. (3) is represented by the area enclosed between the loading and the unloading curves in the load-displacement plot. Fig. 9a compares the cyclic response of the two configurations, after the first loading cycle. A significant increase in the total energy dissipation capability is noticed, if normalized to the mass in Fig. 9b. This improvement is strongly desired when discussing the beneficial effect of a secondary material filled inside a primary external thin shell, and it is easily explained considering what previously discussed in paragraph 3.1 and the good hysteretic properties of the PU foam, not a rare feature among hyper-elastic materials.

The SED gains more than 18% by the presence of the foam; the SDC increases of more than 6%. This last value is obviously not impressively high because, as seen in Fig. 9a, the unloading response is really similar in the two configurations: the FF increased load bearing capacity compared with the empty configuration provides the same increment in the TED and TEA so the effective SDC enhancement is not allowed to reach such impressive values.

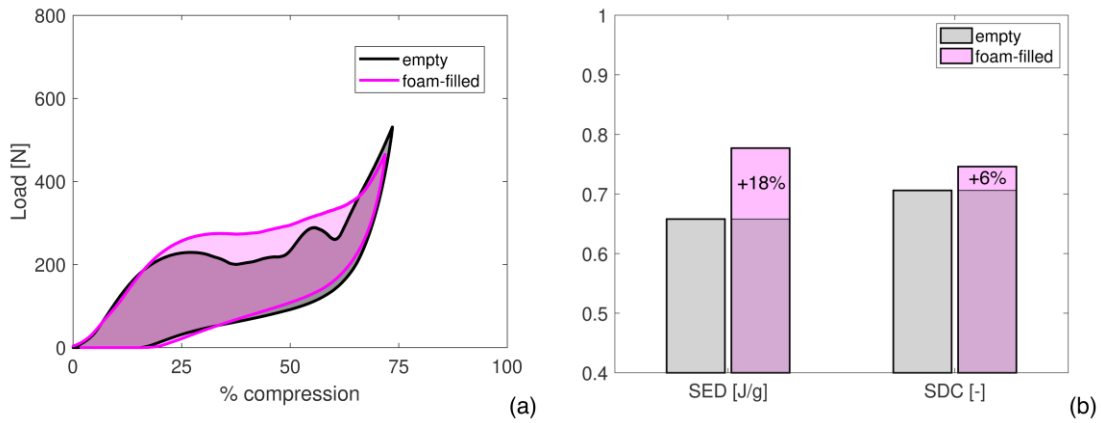

Figure 9: a) Cyclic loading in empty and FF configurations; b) Influence of foam-filling on SEA and SDC.

3.3 Results scalability

Both the checks previously discussed in section 2.5 provided successful results: Fig. 10b proves that the TEA per unit cell is almost independent of the number of cells when considering a 2x2x2 and a 3x3x3 cells structures, see Fig. 10a, which means the structure is scalable and the behavior does not change significantly with the size. In details, the effect of foam-filling is similar for all the configurations, enhancing the energy absorption capability of an average 17%.

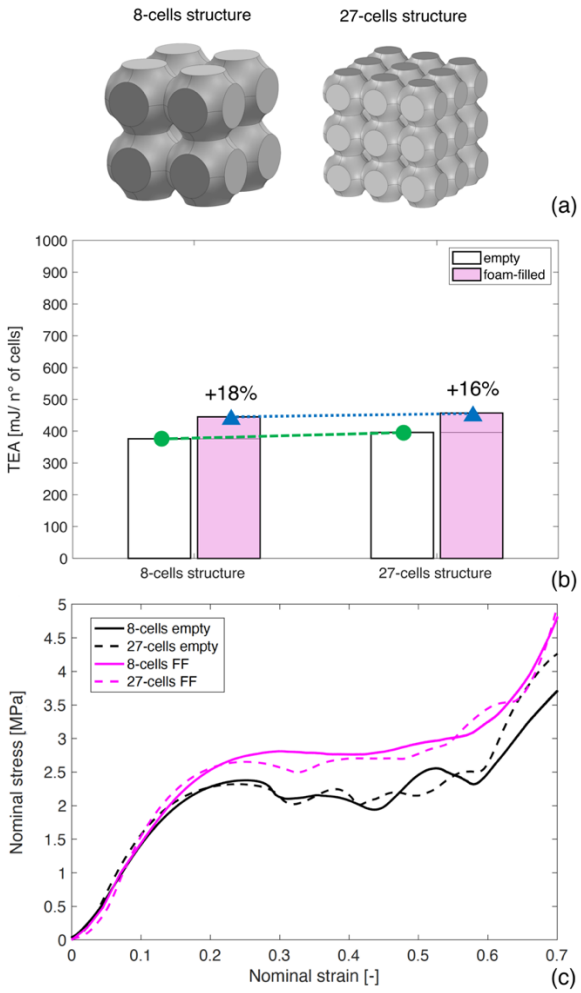

Figure 10: Scalability of the cellular structure: a) Geometry of the specimens; b) Energy absorption per unit cell; c) Initial stiffness and plateau stress for different sizes.

The initial stiffness is also constant, allowing to neglect a scale-effect in the compressive response, as for small nominal strain the structure behaves as a elastic linear spring. Moreover, also the plateau stress results to be independent from the number of cells, and confirms the desiderable increase when the secondary material is injected, see Fig. 10c. The average plateau stress in the FF configuration, defined as the mean of the plateau stresses of the 8-cells and 27-cells structures, is about 30% higher than that of the original configuration.

This is an encouraging result as it proves that the foam on one side delays the occurrence of plasticity in the external shell material, and on the other side reduces the anisotropy, becoming more regular and uniform.

Finally, the obtained experimental results for the FF meta-material and the original cells, are reported in a Ashby map relative to the Specific Energy Absorbtion performance of engineering materials, with respect to their density, see Fig. 11. Present data points falls within the region of lattices, and, specifically, locate at the top performance level for non-metallic materials. This confirms the advatanes in applying such structures.

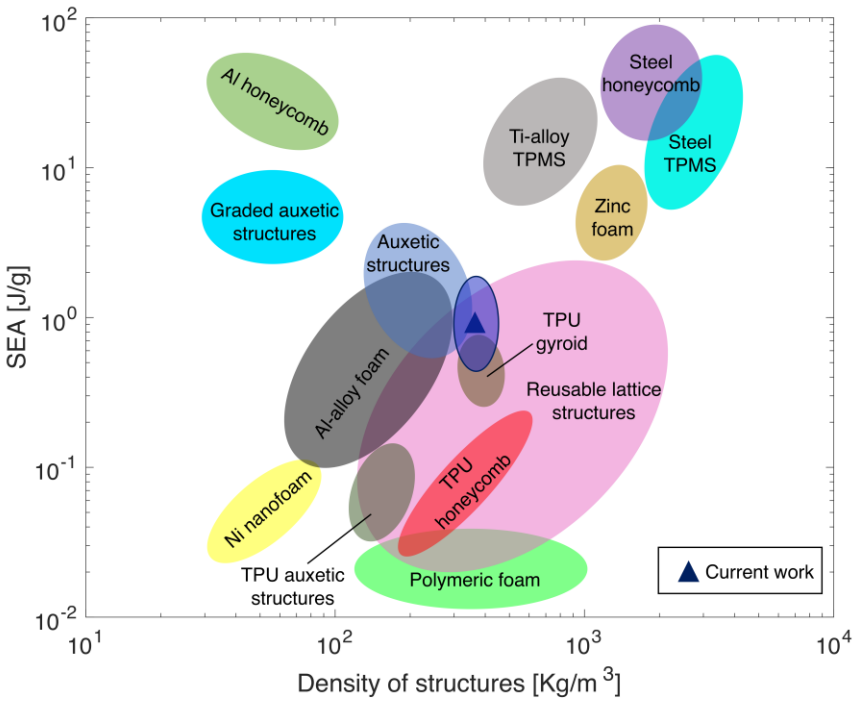

Figure 11: Ashby map with current and literature data points, from [44].

4. CONCLUSIONS

In this work the effect of the injection of a secondary, soft material on the compressive response of a biopolymeric lattice structure is investigated. Comparing the mechanical response of the original, non-hybrid, configuration with the PU expandable foam-filled one, positive results are found for both the static and cyclic behavior. Numerical simulations support experimental tests with excellent agreement, demonstrating the reproducibility of the compressive response and giving tips for understanding the stresses distributions and their influence on the deformation that is ruling the whole structure. Also, the scalability of the structure is demonstrated, bringing results to a more general theory and to a wider field of application.

In conclusion, major findings of the work can be listed as follows:

- PBAT confirms good mechanical properties and good printability, paving the way to a more environmentally sustainable production thanks to its demonstrated biodegradability;
- filling thin-walled structures with a secondary foam-like material brings a desirable increase in the compressive response thanks to an interaction effect raising between the two constituents, that combines the good properties of additively manufactured lattices and the functional effect of the PU foam;
- foam-filled periodic structures show a more uniform and regular deformation when subjected to compression, contrasting the buckling of some cells-layers which are responsible of a drop in the supported load;
- the effect of the foam is extremely benefic both when considering the overall load-bearing capacity and the energy absorption capability: the plateau stress is 30% increased and the average SEA 18% greater;
- the new functionalized meta-material performs among the best lattices.

Moreover, the proved bio-degradability of PBAT polymer and the good mechanical behavior could pave the pathway to new fields of applications for 3D-printed mechanical metamaterials, for example the food packaging industry needing energy absorbers and dumpers towards a green plastic-free transition, or the biomechanic field where the biodegradability is a very desiderable aspect for scaffolds in tissue rigeneration applications.

Future works will compare different TPMS and lattice geometries, to evaluate how the foam contribution relates with the ammount of local deformation in different bending- or stretch-dominated structures.

Acknowledgments

This work is in the framework of the Project funded under the National Recovery and Resilience Plan (NRRP), Mission 4 Component 2 Investment 1.5 - Call for tender No. 3277 of 30/12/2021 of Italian Ministry of University and Research funded by the European Union – NextGenerationEU – Award Number: Project code ECS00000033, Concession Decree No. 1052 of 23/06/2022 adopted by the Italian Ministry of, CUP D93C22000460001, "Ecosystem for Sustainable Transition in Emilia-Romagna" (Ecosister).

REFERENCES

[1] J. Fan, *et al.*, A review of additive manufacturing of metamaterials and developing trends, *Materials Today*, 50 (2021) 303-328.

[2] D. Sharma and S. S. Hiremath, Additively manufactured mechanical meta materials based on triply periodic minimal surfaces: Performance, challenges, and application, *Mechanics of Advanced Materials and Structures*,

[3] R. Miralbes, et al., Characterization of additively manufactured triply periodic minimal surface structures under compressive loading, *Mechanics of Advanced Materials and Structures,*

[4] R. Noroozi, et al., Additively manufactured multi-morphology bone-like porous scaffolds: Experiments and micro-computed tomography-based finite element modeling approaches, *International Journal of Bioprinting*, 8(3) (2022) 556.

[5] B. Yilmaz, Additive manufacturing and characterization of mathematically designed bone scaffolds based on triply periodic minimal surface lattices, *Mechanics of Advanced Materials and Structures,*

[6] J. Li, et al., Topology optimisation of anisotropy hierarchal honeycomb acoustic meta materials for extreme multi-broad band gaps, *Mechanics of Advanced Materials and Structures,*

[7] J. U. Surjadi, *et al.*, Mechanical metamaterials and their engineering applications, *Advanced Engineering Materials*, 21(3) (2019) 1800864.

[8] S. Shan, et al., Multistable architected materials for trapping elastic strain energy, *Advanced Materials*, 27(29) (2015) 4245-4383.

[9] F. Ghorbani, et al., Investigation of energy absorption performances of a 3D printed fibre-reinforced bio-inspired cellular structure under in-plane compression loading, *Mechanics of Advanced Materials and Structures*,

[10] Y. Chen, et al., Multi-material topology optimisation of micro-composites with reduced stress concentration for optimal functional performance, *Materials & Design,* 210 (2021) 110098.

[11] D. H. Werner, *et al.*, Nature inspired optimization techniques for metamaterial design. In: Diest, K. (eds) Numerical Methods for Metamaterial Design. Topics in Applied Physics, vol. 127. Springer, Dordrecht.

[12] A. Corvi, *et al.,* Analysis and modelling of damage mechanism in FDM 3D-printed lattice structure under compression loading, *Journal of Mechanical Science and Technology*, 37(3) (2023) 1089-1095.

[13] A. Kumar, *et al.,* Design and additive manufacturing of closed cells from supportless lattice structure, *Additive Manufacturing*, 33 (2020) 101168.

[14] L. Collini, *et al*., Design and optimization of 3D fast printed cellular structures, *Material Design and Processing Communications* 3(4) (2021) e227.

[15] Z. Huang, et al., Mechanical properties and energy absorption performance of bio-inspired dual architecture phase lattice structures, *Mechanics of Advanced Materials and Structures*,

[16] G. Dong, *et al.,* Design of shoe soles using Lattice Structures fabricated by Additive Manufacturing, in *Proceedings of the 22nd International Conference on Engineering Design (ICED19)*, Delft, The Netherlands, 5-8 August 2019.

[17] J. J. Andrew, *et al.*, Impact behavior of nanoengineered, 3D printed plate-lattices, *Materials and Design*, 202 (2021) 109516.

[18] Y.-T. Kao, *et al.,* Low-velocity impact response of 3D-printed lattice structure with foam reinforcement, *Composite Structures*, 192 (2018) 93-100.

[19] M. Khodaei, et al., Numerical investigation of high velocity impact on foam-filled honeycomb structures including foam fracture model, *Mechanics of Advanced Materials and Structures*,

[20] H. Yin, *et al.,* Crashworthiness optimization design for foam-filled multi-cell thin-walled structures, *Thin-Walled Structures*, 75 (2014) 8-17.

[21] A. Ghamarian, Experimental and numerical crashworthiness investigation of empty and foam-filled end-capped conical tubes, *Thin-Walled Structures*, 49 (2011) 1312-1319.
[22] H. Mozafari, Finite element analysis of foam-filled honeycomb structures under impact loading and crashworthiness design, *International Journal of Crashworthiness*, (2016) 1140710.
[23] R.-Y. Yao, *et al.*, Energy absorption behaviors of foam-filled holed tube subjected to axial crushing: Experimental and theoretical investigations, *Mechanics of Advanced Materials and Structures,* 28 (2021) 2501-2514.
[24] A. Farrokhabadi, et al., Investigation of the energy absorption capacity of foam-filled 3D-printed glass fiber reinforced thermoplastic auxetic honeycomb structures, *Mechanics of Advanced Materials and Structures,* 30(4) (2023) 758-769.
[25] F. H. Roudbeneh, *et al.*, Experimental investigation of quasistatic penetration tests on honeycomb sandwich panels filled with polymer foam, *Mechanics of Advanced Materials and Structures*, 27(21) (2020) 1803-1815.
[26] S. Black, et al., Mechanical behaviour of gel-filled additively-manufactured lattice structures under quasi-static compressive loading, *Materials Today Communications*, 35 (2023) 106164.
[27] G. Lin, et al., Low velocity impact response of sandwich composite panels with shear thickening gel filled honeycomb cores, *Composites Communications*, 32 (2022) 101136.
[28] S. She, et al., Investigating the dynamic compression response of elastomeric, additively manufactured fluid-filled structures via experimental and finite element analyses, *Additive Manufacturing*, 39 (2021) 101885.
[29] Z. Wang, et al., Flexible impact-resistant composites with bio-inspired three-dimensional solid-liquid lattice designs, *Applied Materials & Interfaces*, 15 (2023) 22553-22562.
[30] N. V. Gama, et al., Polyurethane foams: Past, Present, and Future, *Materials*, 11(10) (2018) 1841.
[31] T. Liu, et al., Mechanical characteristics and foam filling enhancement mechanism of polymeric periodic hybrid structures under uniaxial compression, *Materials & Design*, 227 (2023) 111762.
[32] R. Yao, *et al.,* A bio-inspired foam-filled multi-cell structural configuration for energy absorption, *Composites Part B*, 238 (2022) 109801.
[33] X. Ren, *et al*., Mechanical properties of foam-filled auxetic circular tubes: experimental and numerical study, *Thin-Walled Structures*, 170 (2022) 108584.
[34] A. Airoldi, *et al.,* Foam-filled energy absorbers with auxetic behavior for localized impacts, *Materials Science & Engineering A*, 788 (2020) 139500.

[35] H. C. Luo, *et al*., Mechanical properties of foam-filled hexagonal and re-entrant honeycombs under uniaxial compression, *Composite Structures*, 280 (2022) 114922.
[36] N. Novak, *et al.*, Bending behavior of triply periodic minimal surface foam-filled tubes, *Mechanics of Advanced Materials and Structures,* 30(15) (2023) 3061-3074.
[37] R. Miralbes, et al., Mechanical properties of hybrid structures generated by additively manufactured triply periodic minimal surface structures and foam, *Mechanics of Advanced Materials and Structures,*
[38] M.J. Prajapati, *et al.,* Multi-material additive manufacturing with lightweight closed-cell foam-filled lattice structures for enhanced mechanical and functional properties, *Additive Manufacturing*, 54 (2022) 102766.
[39] C. Sciancalepore, *et al.,* Preparation and characterization of innovative poly(butylene adipate terephthalate)-based biocomposites for agri-food packaging application, *Journal of Applied Polymer Science,* 139(24) (2022) 52370.
[40] C. Sciancalepore, *et al*., Flexible PBAT-Based composite filaments for tunable FDM 3D Printing, *ACS Applied Bio Materials*, 5(7) (2022) 3219–3229.
[41] L.J. Gibson, M.F. Ashby, Cellular Solids, Cambridge University Press, 1997.
[42] E. Togliatti, *et al.*, Viscoelastic characterization and degradation stability investigation of Poly(butylene-adipate-co-terephthalate) – Calcium-Phosphate Glass composites, *Journal of Polymers and the Environment*, 30(9) (2022) 3914–3933.
[43] A. Pietrosanto, *et al.,* Development of Eco-Sustainable PBAT-Based blown films and performance analysis for food packaging applications, *Materials*, 13(23) (2020) 5395.
[44] D. Sharma, *et al.,* Bio-inspired repeatable lattice structures for energy absorption: Experimental and finite element study, *Composites Structures,* 283 (2022) 115102.